

Computational Simulation of the Dynamic Stability of L4 and L5 Lagrange Points in the Jupiter-Sun System

Cambridge University

Abstract

Lagrange points L4 and L5 in the Jupiter-Sun system were investigated by means of a numerical simulation of a two dimensional restricted 3-body problem in a co-rotating reference frame. Numerical techniques were analysed and justified within the given limitations. One-dimensional stability analysis for the Jupiter-Sun system showed a narrow symmetric region of stability at $5.197 \pm (0.131 \pm 0.006) AU$ in the radial direction and wider asymmetric region of angular stability. Similar behaviours were seen for the Mars-Sun and Earth-Sun systems. Two dimensional analyses yielded a characteristic symmetric tear-drop shaped region of spatial stability (Area = $1.705 AU^2$) in polar coordinates. Stability in velocity space was also found to be consistent with spatial findings. Extending the simulation onto systems with different mass ratios yielded an upper threshold of $\mu = 0.04$ for dynamic stability of L4, in excellent agreement with previous literature.

Keywords: Trojan Asteroids, Lagrange Points, Dynamic Stability, Mass Ratios

1. Introduction

The Trojans are a large group of asteroids that share an orbit with Jupiter around the sun. That is, in a rotating reference frame in which Jupiter and the Sun are at rest, the Trojans remain in essentially fixed positions, performing small librations about a central point of stability, known as the Lagrange Point L4 [1].

Lagrange points arise from analytical treatment of a restricted 3-body problem (one where a third body's mass is negligible compared to the masses of the other two ¹), in a co-rotating reference frame. In such a system, five Lagrange points are found to exist, all corresponding to the locations of stationary points in the effective potential of the restricted 3-body system. None of these points actually lie at energetical minima (L1-L3 are saddle points and L4 and L5 are maxima, See Fig.1), suggesting that they should not be dynamically stable, and indeed the L1-L3 points are found to be unstable. Curiously, however, the two maxima (L4 and L5), actually display significant stability. This is because any displacements from these

¹This assumption is valid for the Trojan asteroids as their combined mass is approximately 3×10^{-7} that of Jupiter's[2]

points of stability incurs an increase in velocity which then curves (due to the Coriolis force), to create what is known as a Lissajous orbit around the stationary point [3].

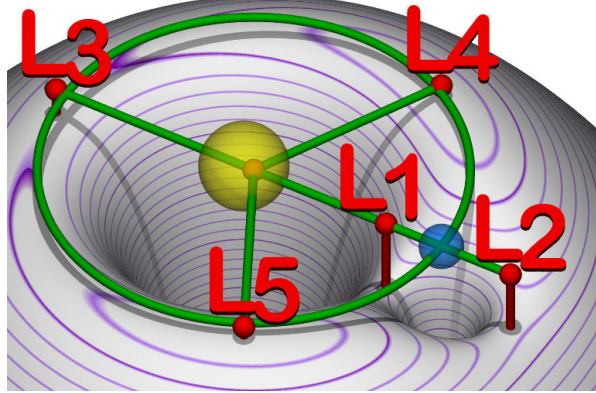


Figure 1: 3D contour plot of effective potential and locations of Lagrange points 1-5 for the restricted 3-body system being considered in this investigation [4]

Lagrange points are thus of great interest in astronomy as small masses (such as asteroids or satellites) can be positioned there and remain in stable orbits for extended periods of time. L1-L3, while theoretically unstable, can also, with small periodic adjustments, be utilised for their stability. Indeed many satellites are currently positioned at these points in the Earth-Sun system to facilitate various scientific missions including imaging far away systems with less light pollution from the sun at L3.

This report will principally seek to investigate the stabilities of the L4 (and by symmetry, L5) Lagrange points in the Jupiter-Sun system, with comparisons drawn to other systems. In so doing it will aim to:

1. Implement a computational simulation in Python of the restricted 3-body problem and analyse its performance and accuracy in describing orbital motion about the L4 Lagrange point.
2. Examine the effect on stability of small displacements (both in position and velocity space) from the L4 Lagrange point
3. Examine the effect of varying the mass ratio between the larger and smaller masses on the stability of these points.

2. Physical Model

2.1. Coordinate System and Dynamics

To simplify the dynamics without losing much generality, this simulation will exclusively make use of a 2-dimensional Cartesian coordinate system in which the Sun and Jupiter are at rest with respect to the planar rotating reference frame focused on their barycentre (Figure 2).

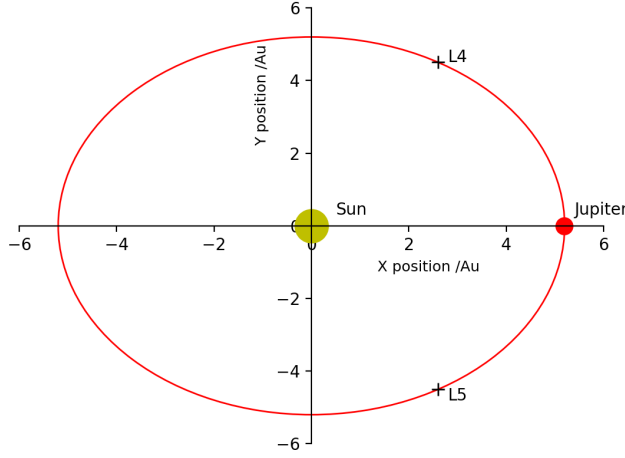


Figure 2: Coordinate system used in this investigation. This reference frame co-rotates with the Sun/Jupiter about their barycentre which defines the origin. The sun is at $[-r_p, 0]$ and Jupiter as at $[r_s, 0]$

In this frame of reference, the relevant equations of motions for a small (negligible) third mass can be shown to be [3]:

$$\ddot{x} = w(wx + 2\dot{y}) + G \left[\frac{M_p(r_p - x)}{(y^2 + (r_p - x)^2)^{\frac{3}{2}}} - \frac{M_s(r_s + x)}{(y^2 + (r_s - x)^2)^{\frac{3}{2}}} \right] \quad (1a)$$

$$\ddot{y} = w(wy + 2\dot{x}) + Gy \left[\frac{M_p}{(y^2 + (r_p - x)^2)^{\frac{3}{2}}} - \frac{M_s}{(y^2 + (r_s - x)^2)^{\frac{3}{2}}} \right] \quad (1b)$$

Where M_p , r_p and M_s , r_s are the masses and distances from a common barycentre of the planet and sun, respectively, and $w = \sqrt{\frac{G(M_p+M_s)}{R^3}}$ is the angular velocity of the rotating frame. To ensure some physical realism, the simulation will make use of the following units and measurements for the Jupiter-Sun system:

Table 1: System Units

Quantity	Unit
Length	AU
Mass	M_\odot
Time	Earth Year

Table 2: Constants for Jupiter Sun System

Constant	Value
R	5.2
M_p	0.001
G	$4\pi^2$

2.2. Locations of Lagrange Points

The location of the Lagrange points can be found by subjecting the equations of motions to the constraints of zero velocity and acceleration (Eq. 1). This yields a

quintic equation for the L1-L3 points that cannot be solved analytically. In contrast, the L4 and L5 points admit a much more simple analytical treatment, sitting on the the third corner of equilateral triangles with the bottom edge defined by the distance between the centres of the two masses:

$$\mathbf{r}_0 = (r_p - R/2, \pm\sqrt{3}R/2) \quad (2)$$

With the positive solution corresponding to L4 and negative to L5. The high degree of symmetry between these points, however, lets us focus solely on L4 with all discussion extending seamlessly to L5².

3. Implementation

3.1. Design

In designing the computational simulation three core design aims were identified:

1. Readable and reusable code
2. Reasonable precision and accuracy
3. Performance: specifically designed to run in a reasonable time frame on a 2GHz intel core i5 processor

In satisfying the first aim, an object-oriented approach was adopted to ensure multiple parameters could be easily modified and core functionality retained without writing excess code. A class system was constructed in which a class defining an *orbit* containing all the relevant evolution functions, inherited from an *Orbital System* class which defines the system parameters and the relevant equations of motion. This structure then enabled the rest of the program to make use of shorter functions to carry out the various experiments and plot relevant graphs in an intuitive way without much repetition.

The second two aims, as in any computational exercise, proved to often be at odds with each other. Where possible, performance improvements were made through vectorisation and other techniques with no cost to overall accuracy. However, the bulk of computation revolved around integrating the equations of motions using a built in ODE integrator (which could not be vectorised simply). Many of the computations performed in this investigation were quite demanding, requiring thousands of different orbits to be simulated for lengthy periods. Such memory intensive computations also meant that attempting to run multiple simulations in parallel also often resulted in RAM overflow errors. The constant trade-off between spatial and temporal resolution (Section 4.1), and accuracy of integration (Section 3.2) meant that constant adjustments had to be made between different tests to achieve optimal results in reasonable time frames.

²Considerable asymmetry has, in fact, been observed between L4 and L5 [5], with both points having different numbers and mass distributions of asteroids. The origin of this is likely to do with perturbative effects such as that of Saturn and drag of celestial dust [1], and is thus outside the scope of this model.

3.2. Integrators

Solving the equations of motions for this system could be done by breaking them down into 4 coupled ordinary differential equations:

$$\dot{r}_x = v_x \quad (3a)$$

$$\dot{r}_y = v_y \quad (3b)$$

$$\dot{v}_x = \dot{v}_x \mathbf{r}, v_y \quad (3c)$$

$$\dot{v}_y = \dot{v}_y \mathbf{r}, v_x \quad (3d)$$

These equations could then be plugged into a general ODE integrator with a set of initial conditions, and relevant coordinates (x, y, v_x, v_y) extracted for a number of time-steps.

A variety of SciPy ODE Integrator algorithms were examined for their performance and accuracy. Scipy provides two main suites for ODE solving, which for simplicity will be referred to as “ODE” (`scipy.integrate.ode`) and “IVP” (`scipy.integrate.solve_ivp`). IVP is a newer iteration upon the older and now unsupported ODE suite, and contains several important modifications, including adaptive time-step setting. Both suites make use of a variety of integration algorithms (see documentation), to solve both stiff and non-stiff ODE’s. It should be noted that while two integrators can ostensibly use the same algorithms (according to documentation, `odeint` also uses the LSODA ”Adam’s Method” algorithm), their performance and accuracy often still differs due to their internal implementation. Instead of a detailed theoretical analysis of the algorithms and their suitability to this particular problem, an empirical approach was favoured. Each integrator was run for 1000 orbits for stable, slightly perturbed, and completely unstable initial conditions and maximum radial displacement from initial position and time taken for each integrator was inspected (Figure 3).

Figure 3a suggests compelling superiority of integrators (except RK45) within the Solve_IVP Suite relative to the ODE Suite in terms of both accuracy (expected wander should be 0) and performance. However when the initial conditions are perturbed slightly (Figure 3b) there is a marked relative decrease in performance of the Solve_IVP Suite (the Radau integrator in particular has an almost 1000-fold increase in computation time). Radial wanders continue to appear roughly consistent between all integrators except LSODA of the IVP Suite.

While the investigation is concerned primarily with stability, completely unstable orbits will often have to be simulated in order to characterise the stable orbits. These often incur a much higher performance penalty due to their unbounded nature. Figure 3c shows incredibly variable behaviour between different integrators for unstable orbits. The IVP suite now performs exceptionally poorly, taking on average twice as long as the ODE suite (except RK45 which surprisingly copes much better with instability than stability). Wanders were extremely disparate in general, among both suites, despite purportedly using similar algorithms. However this isn’t a major

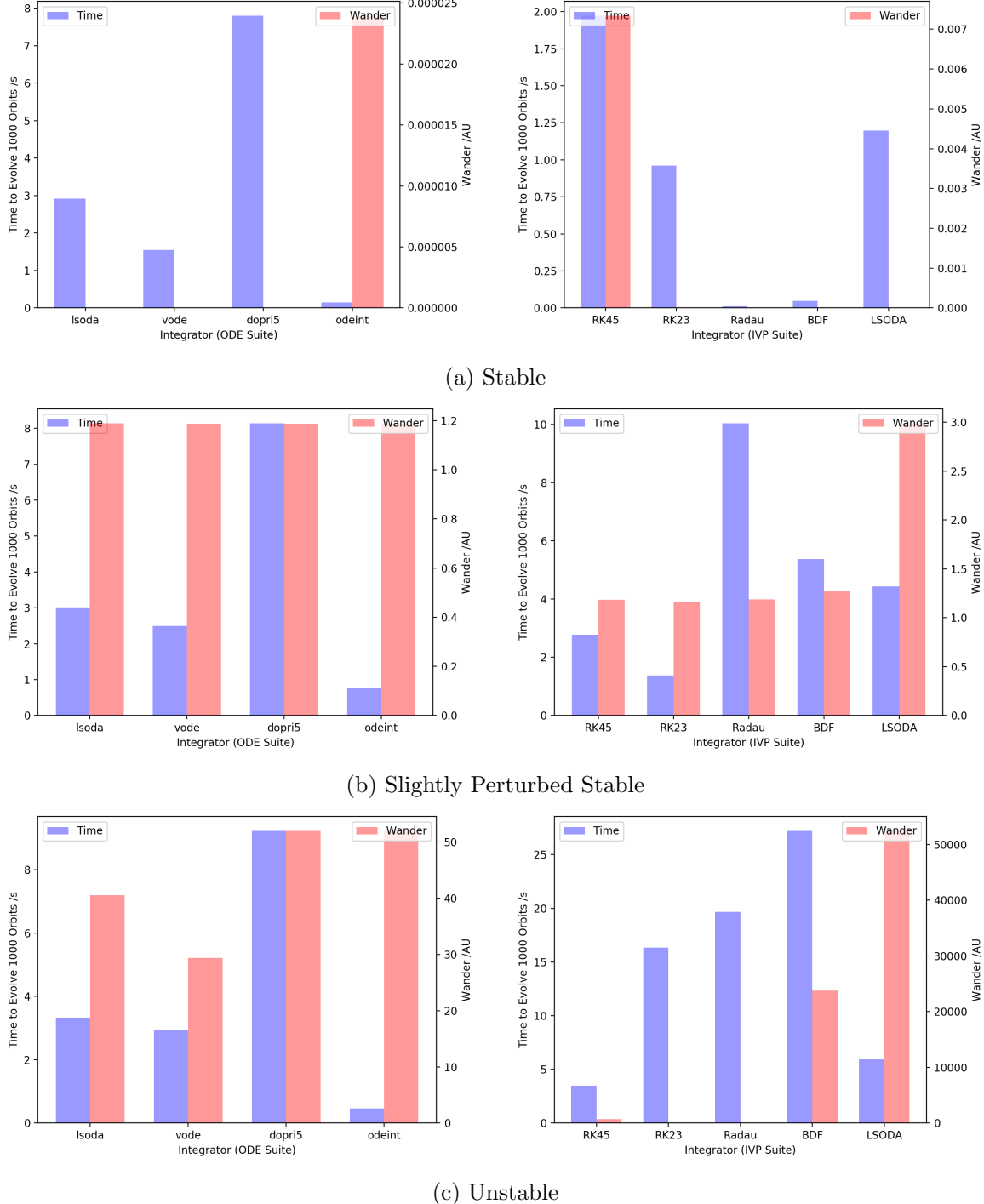


Figure 3: Time taken to evolve 1000 orbits and Radial Wander calculated for (a) stable orbits starting from L4, (b) slightly perturbed (0.01AU radially) stable orbits, (c) unstable orbits(displaced radially by 0.3AU). Orbits are evolved using different integrators from the ODE (left) and Solve_IVP Suite (right).

concern as the degree of instability is not being assessed here, only the occurrence thereof. Due to the inconsistency of the IVP Suite in different regimes, it was thus decided to make use of the ODE suite exclusively.

Within the ODE suite the “dopris5” algorithm was identified as consistently the most accurate, but also by far the slowest. “odeint” was the fastest but somewhat less accurate. Lsoda and vode fell somewhere in between. Due to the varying nature of the tests being performed in this investigation (some requiring greater accuracy, some requiring better performance, some requiring both) a range of integrators from the ODE suite were used throughout this investigation (see Appendix A for a table of integrators and run times for each figure generated).

3.3. Stability Metrics

Quantifying stability reliably proved somewhat challenging in this investigation. What is optimally desired is some measure of the spatial and temporal consistency of an orbit (an autocorrelation function of some form). However due to the difficulty of implementing this in this complex 2 dimensional system, some more simple measures of stability were devised by examining orbital paths. Figure 4 shows a number of example orbits of increasing degrees of instability. (a) and (b) are known as ”tadpole orbits” which have been commonly observed to occur for L4 Trojan asteroids. (c) is known as a ”horseshoe orbit” and while theoretically possible, no asteroid is yet known to perform such an orbit[1].

The most intuitive measure of instability is given simply by maximum displacement from the starting location (radial wander). However this metric can be problematic in that it varies rather slowly over the transition to instability (b to c) and continues to increase rapidly to infinity during instability (d).

A better measure would instead be given by the angle between the leading and trailing edges of an orbit (angular libration). This has the advantage of varying greatly over the transition to instability (more than doubling from (b) to (c)), but reaching a maximum value of 2π for completely unstable orbits (performing full rotations around the origin (d)).

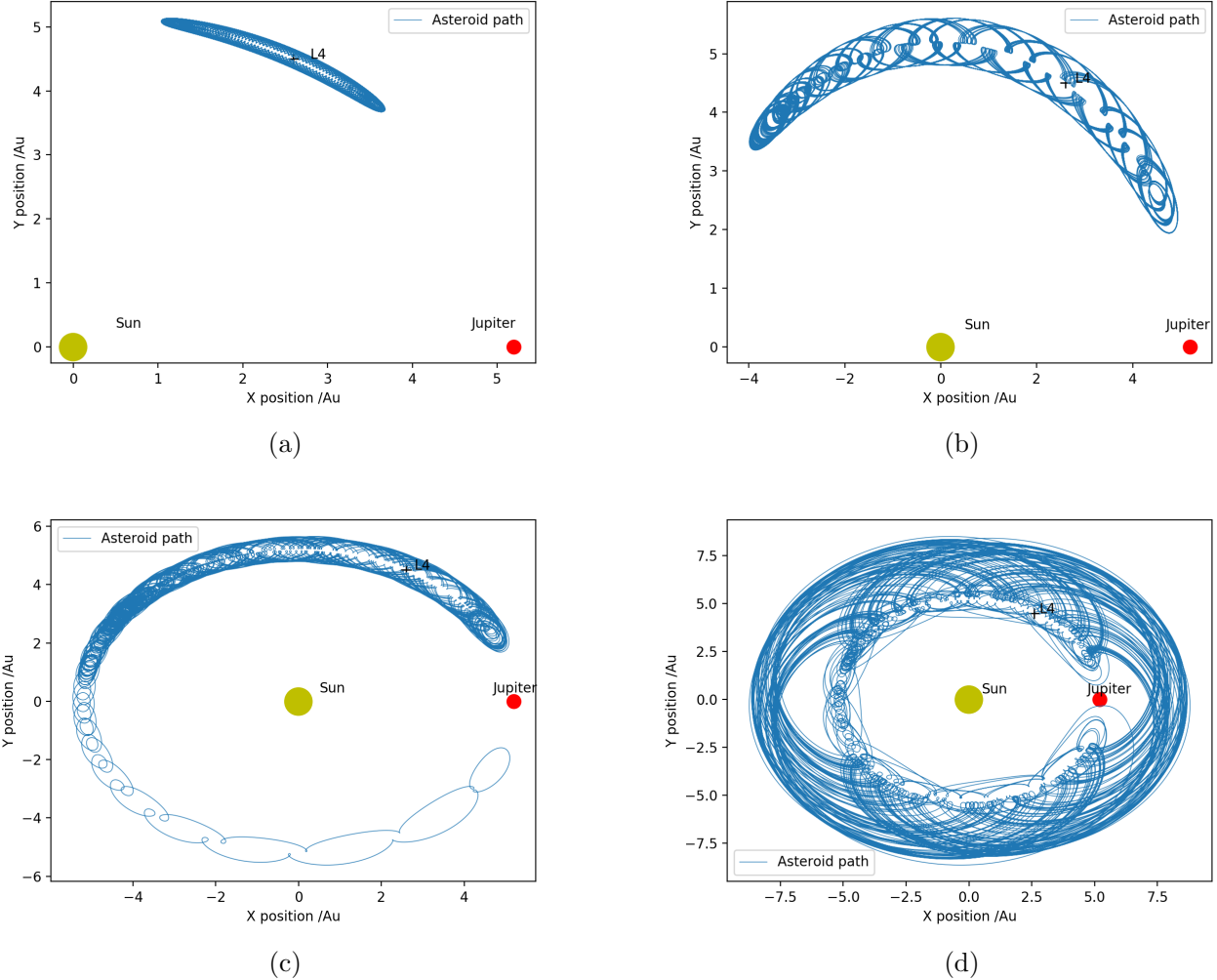


Figure 4: Orbits with different initial conditions of increasing instability (a-d) evolved for 500 orbits each. Orbits (a-c) are stable while d is unstable. Orbits (a) and (b) present the characteristic tadpole shape that characterises closed Lissajous orbits[1] at L4. (c) depicts a horseshoe orbit, a case of borderline stability as the orbit slowly evolves further from L4 until it begins to orbit L5 as well.

4. Results and Analysis

4.1. Temporal Stability

One of the first important things to ascertain is the temporal stability of L4, or more specifically, the minimum number of orbital periods that need to be computed before stability/instability can be correctly designated. This is crucial as the computationally demanding nature of this investigation will mean that running the simulation for large numbers of orbits may become unfeasible. It is thus necessary to determine what might be taken as the lower bound to ensure that accuracy is not compromised when running larger computations.

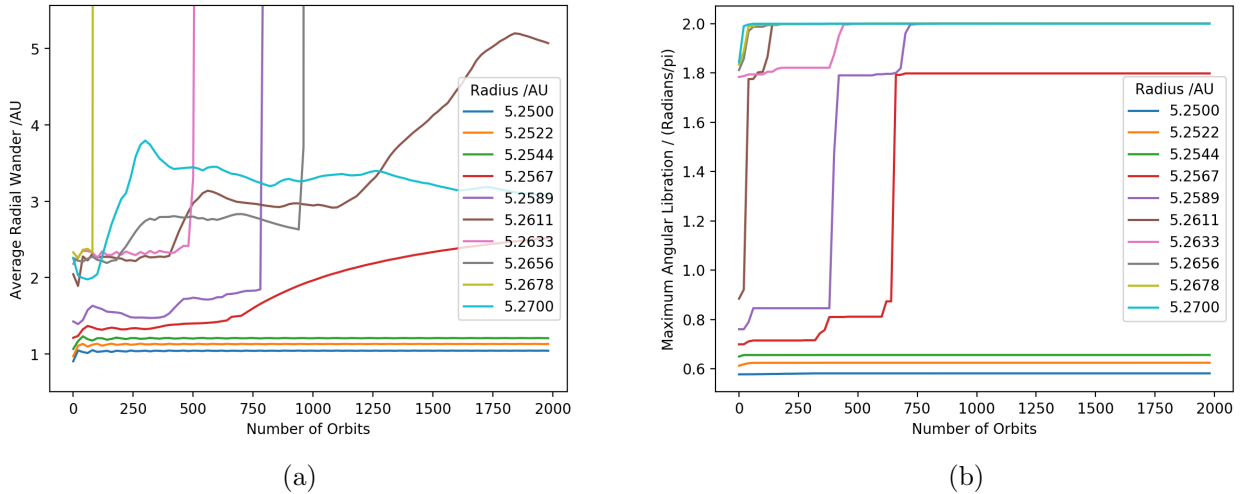


Figure 5: Average radial wander (a) and maximum angular libration (b) computed in steps of 10 for 2000 orbits with different radial initial displacements from L4 around the threshold for instability.

Figure 5 depicts the behaviour of various orbits around a spatial stability threshold. It is clear that while most orbits are markedly either stable or unstable from the very beginning (after 10 Orbits), there are a couple of orbits (purple and red lines) that require as many as 700 orbits to fully transition to instability³. Given that computing this many orbits consistently throughout this investigation exceeds the computing power available, it must be accepted that these will be falsely marked as stable and a range of uncertainty assumed.

To crudely estimate this uncertainty in the radial direction another simulation with a higher spatial and temporal resolution was run (Figure 8) yielding an approximate distance of 6.3×10^{-3} AU over which stability could not be correctly determined

³It is also worthwhile to note here the superiority of the angular libration metric in Figure 5(b) in depicting instability, showing neat vertical transitions followed by plateaus compared to the much more erratic radial wander metric (a).

within 30 orbits or less. This was deemed a reasonable precision for this investigation and so the minimum simulation period was set at 30 orbits for the Jupiter-Sun system (longer periods were used where possible).

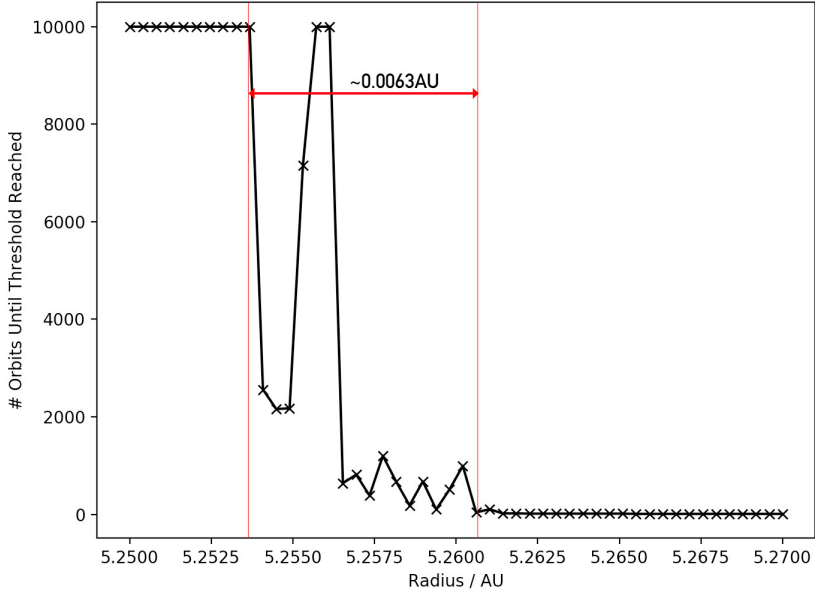


Figure 6: Plot of number of simulated orbits required until threshold instability is reached for orbits with given radii from origin (along radius passing through L4) for the Jupiter-Sun System. Threshold instability is defined somewhat arbitrarily as a maximum angular libration of 1.3π or greater. This definition follows from Fig 5b as the approximate midpoint of the vertical transitions seen. Also note the erratic behaviour near instability.

To assess whether this deduced uncertainty could be applied to different orbital systems, a similar procedure was carried out for the Mars-Sun system, yielding Figure 7(a). Surprisingly, the graph was much better behaved near instability, showing a clear vertical drop at 1.5244AU. However, upon closer examination (Figure 7(b)), it became clear that unlike in the Jupiter-Sun system, there is a characteristically long and potentially asymptotic decline in the number of orbits required to reach threshold instability. This means that a margin of uncertainty method, like that adopted for the more chaotic Jupiter-Sun system, is unfeasible, and instability can only be accurately characterised for simulation periods of approximate 300 Orbits or more. This makes large computations for the Mars-Sun and similar system difficult and very computationally demanding.

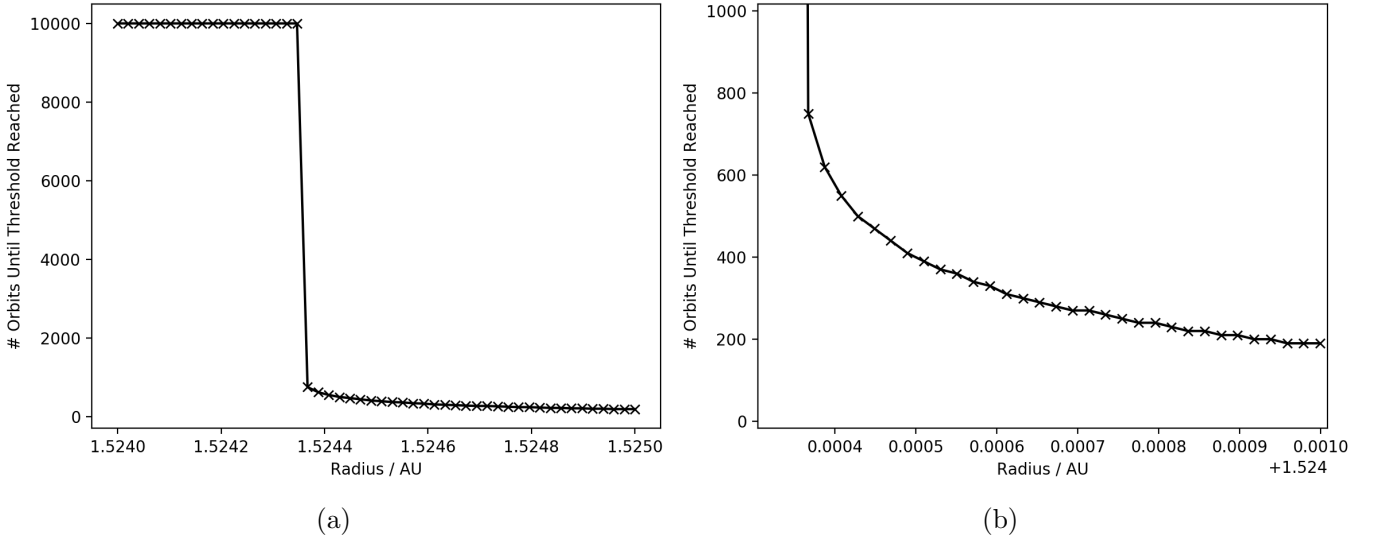


Figure 7: (a) Plot of number of simulated orbits required until threshold instability (defined as an angular libration of 1.2π or greater) is reached for orbits with given radii from origin (along radius passing through L4). (a) has been expanded in (b) to better depict the behaviour after instability. This is for the Mars-Sun system.

4.2. Spatial Stability

4.2.1. In One Dimension

When working with the most accurate integrators (dopri5, a runge kutta method, see section 3.2), orbits originating exactly from L4 yield exactly zero wander. However, when the initial conditions are perturbed so that the starting location is slightly displaced, there is a gradual shift in the stability of the orbits. In order to analyse this spatial stability, a one-dimensional search was first performed, both radially through L4 and along the arc describing the circle on which it lies. Maximum angular libration was used to analyse the wander of orbits from their initial positions. Odeint was the chosen integrator as the experiment was computationally demanding (usually 1000 simulations of 50 orbits each).

For the radial search (Figure 8), a clear symmetric minimum in wander was observed at $5.197AU$ in exact correspondence with the calculated position of L4. The total width of stability was measured to be $0.131 \pm 0.006AU$ (with error derived in section 4.1). While this is not consistent with some observed estimates of the position and width of the Trojan belt ($5.2 \pm 0.15AU$ [5]), many analytical and numerical analyses [6] have similarly under-estimated the apparent size of the Trojan region⁴.

⁴The cause likely has to do with the assumptions of the mathematical model (not accounting for gravitational influences from within the belt, perturbations from other solar planets etc.)

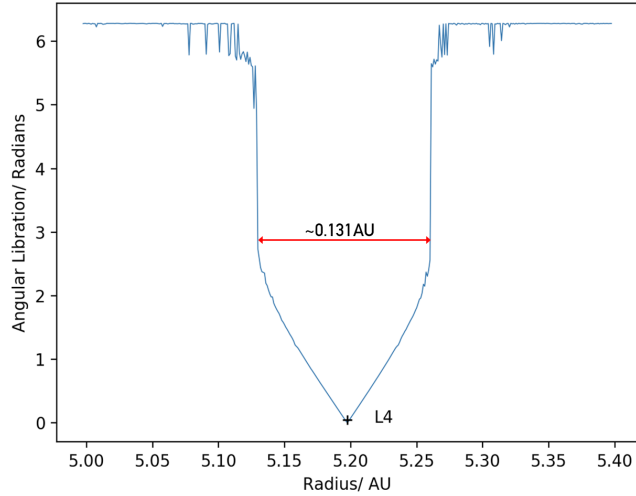


Figure 8: Initial radial position against the maximum angular libration measured over 50 orbits for Jupiter-Sun system. Red line gives width of radial stability.

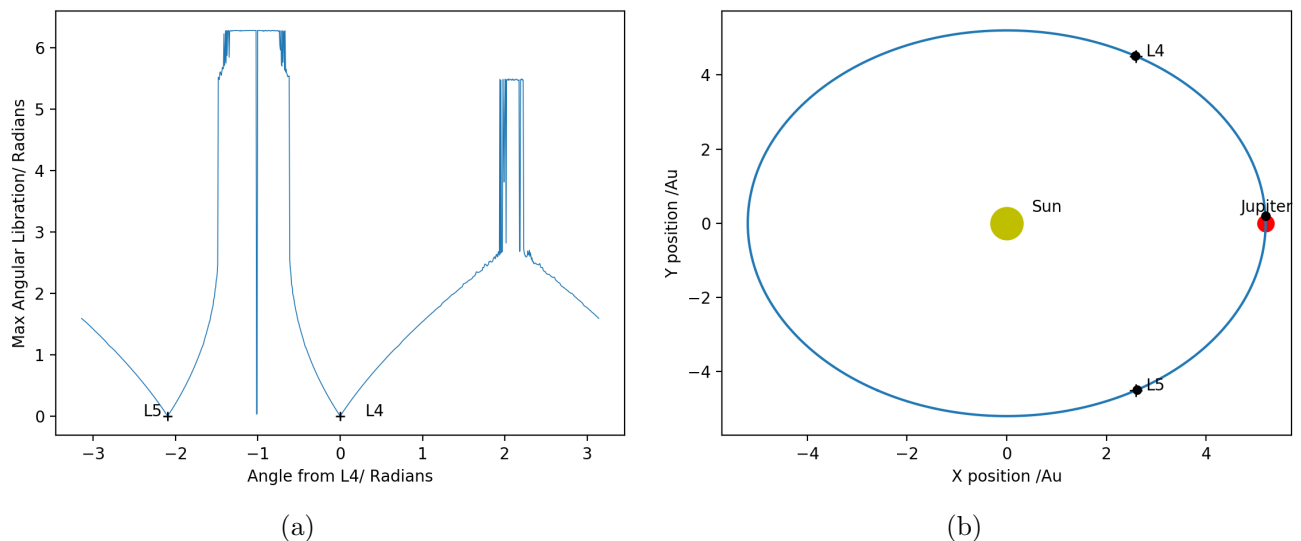


Figure 9: (a) Initial Angular displacement from L4 against the maximum angular libration measured over 50 orbits for Jupiter-Sun system. (b) Stable points found (black dots) plotted on coordinate system.

The angular search (Figure 9) again showed essentially exact correspondence (within stepsize) between position of minima and L4 and L5. The behaviour was markedly less symmetric about L4 however, due to the presence of Jupiter nearby which increased the rate of instability onset dramatically. Near exact symmetry was however observed between L4 and L5, as expected. There was also a third stable minimum observed very near to Jupiter. Upon further examination however it was determined that this was an erroneous result caused by integrator failure in close proximity to Jupiter.

For comparison a similar series of plots were generated for the Mars-Sun (Figure 10), and Earth-Sun (Figure 11) systems. Both of these had to make use of much larger simulation periods (see section 4.1) of 800 orbits each. The resulting radial plots (a) were largely similar in character to that of the Jupiter-Sun system, except, of course, for the width of stability. They also exhibited largely similar angular search plots (b), except for their behaviour around the opposite side of the sun (≈ 2 Radians). While the Earth and Jupiter systems both have maxima in this vicinity, curiously in the Mars-Sun system, a third minimum was observed here. Closer inspection could not easily identify an integrator fault as the root cause, however no physical reason for this apparent stability could be found in previous literature either. Further investigation would thus be of interest here.

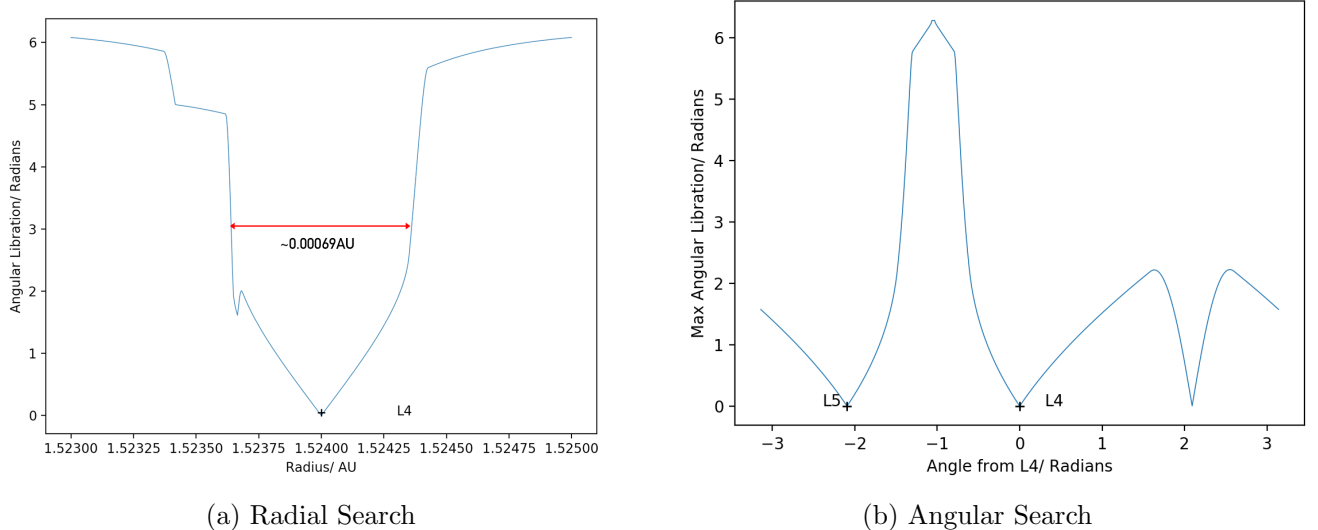
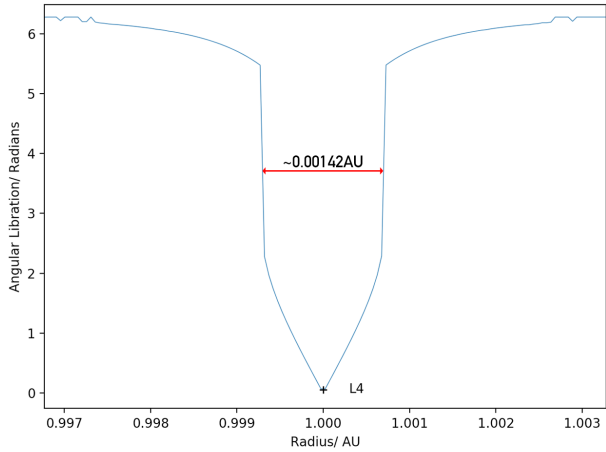
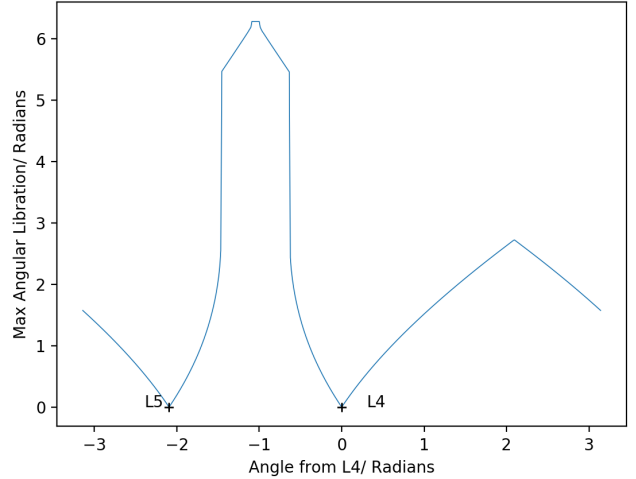


Figure 10: Radial (a) and Angular (b) stability searches for the Mars-Sun system. Simulated for 800 Orbits each.



(a) Radial Search

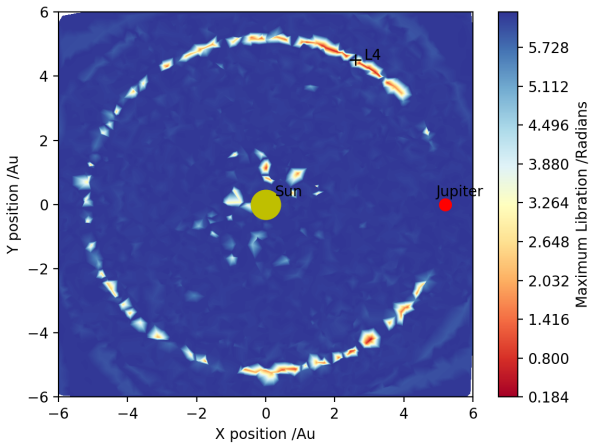


(b) Angular Search

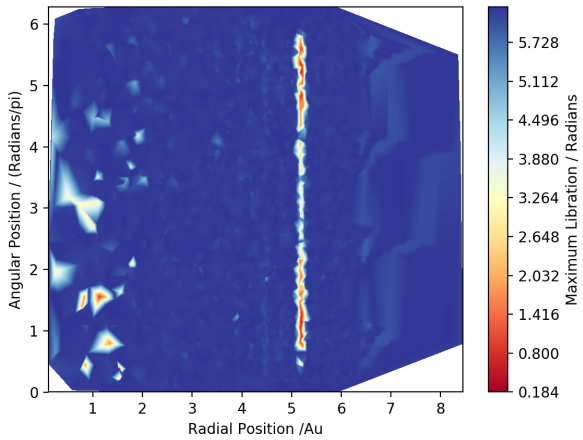
Figure 11: Radial (a) and Angular (b) stability searches for the Earth-Sun system. Simulated for 800 Orbits each.

4.2.2. In Two Dimensions

In order to explore spatial stability more broadly a 2D search was performed. A simple random sampling approach was initially undertaken in order to sample the entire space of interest (Figure 12).



(a) Cartesian Coordinates



(b) Polar Coordinates

Figure 12: Plot of stability in terms of maximum angular libration for 5000 initial positions sampled randomly across the entire area of interest. Shown in (a) cartesian coordinates and (b) polar coordinates. Also note artefacts in close proximity to sun, which are likely due to integrator faults as opposed to any real physical stability.

While the random sampling technique gives a general sense of the area of interest, its noise and need to use rectilinear sampling spaces limits its value. To explore

the apparent ring of stability more systematically, a grid sampling technique was employed that allowed for more successful interpolation methods (particularly of curved spaces) and smoother contours (Figure 13).

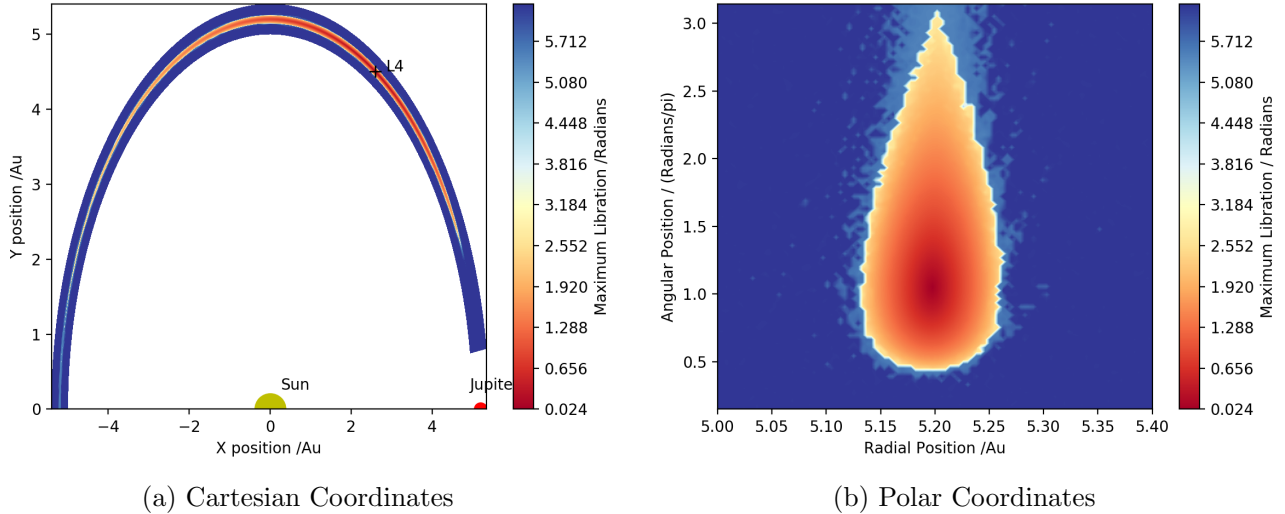


Figure 13: Plot of stability in terms of maximum angular libration for a various initial positions sampled on a grid set in polar coordinates (b) around the area of interest for L4. (a) shows sampling grid in system coordinates.

Figure 13(b) depicts a very well defined area of stability with a high degree of symmetry. The region is drop shaped and has an area of approximately $1.705AU^2$. It conforms well to the shape expected from the 1-dimensional traversals of stability: a thin symmetric radial component and a much wider asymmetric angular component. It also is highly consistent with other empirical and computation models of the Jupiter L4 Lagrange point [1][3].

4.3. Velocity Space Stability

So far we have only examined the spatial aspect of the effect of initial conditions on orbital stability. Much literature has been dedicated to the analysis of the origin of the Jupiter Trojans, including mechanisms and conditions for asteroid capture. A basic treatment of this can be attempted by varying initial velocities for orbits starting from L4 and examining the effect on stability. A 2D grid search was thus performed for initial velocities traversed in both Cartesian and polar coordinates (Figure 14)

The resulting plot depicts a very interesting curved region of stability in velocity space. The polar plot (b) is somewhat more intuitively explained as it suggests a much greater range of initial angular velocities maintaining stability relative to radial velocities, corresponding to the observed smaller width of stability in the radial

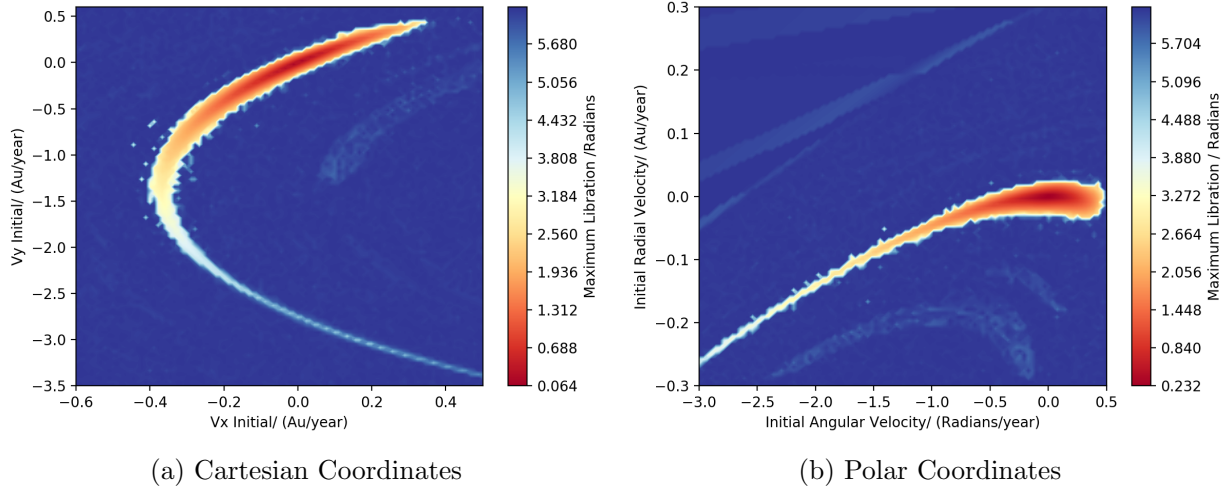


Figure 14: Plot of stability in terms of maximum angular libration for a various initial velocities sampled on a grid set in Cartesian (a) and polar coordinates (b).

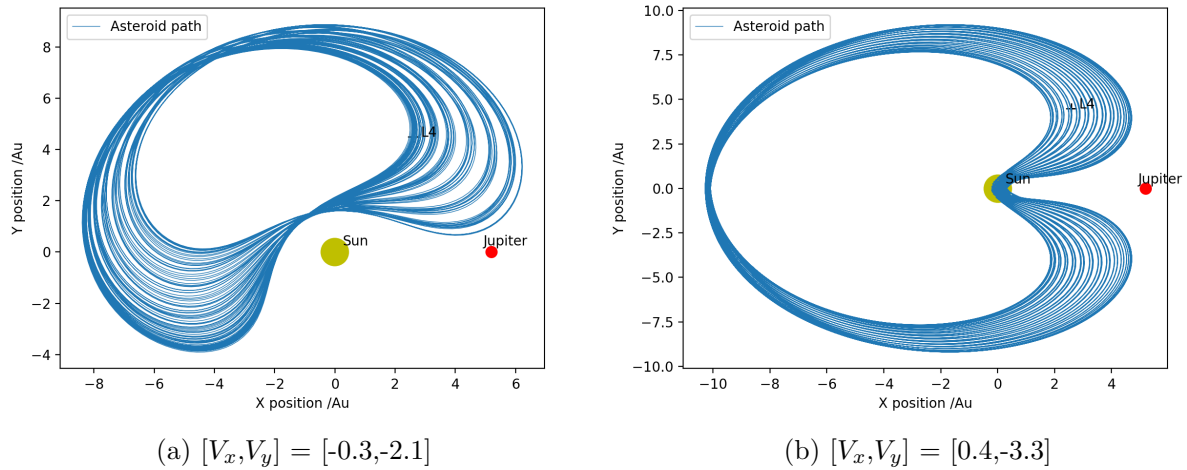


Figure 15: Orbits with different initial velocities evolved for 100 Orbits each. Both appear, in some sense, stable although do not follow the Lissajous orbits expected for L4 Asteroids.

direction. The curved thin tail of both plots is however less intuitive, and indeed orbits with these initial conditions produce extremely interesting orbits (Figure 15).

It is thus possible to envision how asteroids and other celestial objects may be captured by these Lagrange regions even with some substantial initial velocity upon entry, provided it is in a suitable direction.

4.4. Mass Ratio Threshold

We have shown that stable orbits exist not only for Jupiter and its trojan Asteroids, but also for the less massive Earth and Mars, albeit with smaller stability windows. It might be naively supposed that this stability extends on to larger

masses as well. However, early analytical investigations by Gascheau(1843) and later Routh(1875) have suggested that there is a theoretical limit to the mass ratio between the smaller and larger masses in order for the L4 and L5 Lagrange points to remain points of stable equilibrium [7]. To investigate this, mass ratio⁵ was varied and effect on stability for orbits starting from L4 investigated (Figure 16).

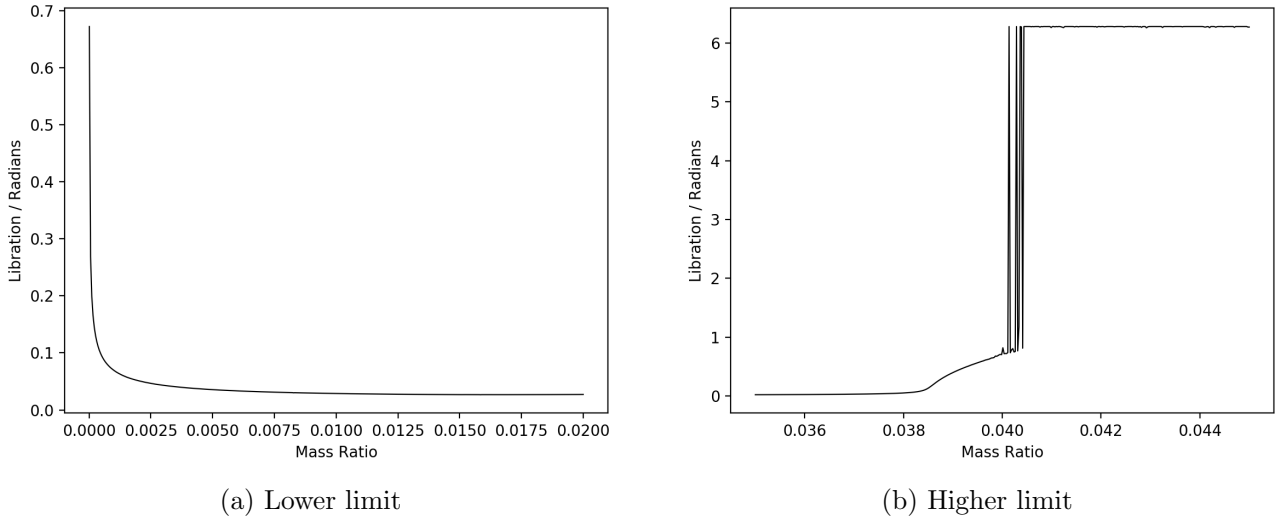


Figure 16: Plot of maximum angular libration as a function of mass ratio for the (a)lower and (b)higher limits simulated for 500 orbits starting from L4.

Gascheau analytical upper limit for stability was quoted as $\mu = 0.03852$ [7]. In Figure 16(b), this point signifies the beginning of a gradual increase towards instability, but total instability is not reached until $\mu = 0.0400$. These values are, in fact, in excellent agreement with analysis performed by Sicardy [7], which found similarly that Gascheau value was only the first in a series of critical values that signal changes in orbital behaviours around L4. Sicardy also observed that $\mu \approx 0.04$ was the true limiting value for total instability, and similarly observed chaotic behaviour around this transition point as seen in Fig. 16(b).

In the lower limit of mass ratios (Fig. 16(a)), there appears to be a smooth asymptotic increase towards instability as $\mu \rightarrow 0$. The likely explanation for this is that the assumption that the third mass (the asteroid) is negligible is voided in this limit, and so the equations of motions used in this simulation become invalid.

⁵Note that, for consistency with literature, mass ratio was defined as $\mu = \frac{M_p}{M_p + M_s}$ where $M_p + M_s = 1$

5. Conclusion

The computational simulation of a restricted 3-body system in a co-rotating frame of reference developed in this investigation was able to model the stability of Lagrange point L4 and, by symmetry, L5, in the Jupiter-Sun as well as Earth-Sun and Mars-Sun systems with a reasonable degree of accuracy and consistency with literature. While limited computing power meant that demanding simulations had to be simulated with shorter integration times, their validity was justified by examining temporal stability of orbits near instability and assuming an error.

One dimensional stability examinations yielded a symmetric narrow region of radial stability of $5.197 \pm (0.131 \pm 0.006) AU$, and a much wider asymmetric region of angular stability. Similar relationships were observed for the Mars-Sun and Earth-Sun systems, with smaller radial widths of stability.

A two-dimensional plot of stability also showed a high degree of consistency both with earlier plots and previous literature, forming a "tear-drop" shaped region of stability in polar coordinates of area $1.705 AU^2$. The effect of varying initial velocity was largely consistent with earlier spatial stability plots, but also led to the discovery of some interesting high energy orbits with curious forms.

The extension of the stability analysis of L4 to different mass ratios saw excellent agreement with Siccardy's [7] observation that the transition to instability begins at Gascheau value of $\mu = 0.03852$, and completes at $\mu = 0.04$ with completely chaotic orbits.

6. Limitations and Further Work

This investigation suffered principally from a lack of computing power and the constraints imposed by adherence to the simplified mathematical model of restricted 3-body problem in a co-rotating reference frame. This meant that true orbital paths in stationary reference frames could not be simulated and more empirical measures of orbital stability and character (orbital inclination and stability), could not be calculated or compared with literature. It also meant that multiple bodies could not be simulated concurrently which likely led to some of the numerical inconsistencies observed with previous empirical literature (section 4.2.1).

Well within the scope of the current limitations and techniques, however, would be an analysis of the L1-L3 Lagrange points and their respective stabilities. While not dynamically stable, it is possible to achieve some considerable spatial and temporal stability via periodic adjustments in velocity (a rocket's boosters). Adding such adjustments into the current simulation would be straightforward, and this area is of great interest to modern astrophysics.

References

- [1] F. Marzari, H. Scholl, C. Murray, C. Lagerkvist, Origin and evolution of trojan asteroids (2002), Asteroids III.
- [2] D. C. Jewitt, C. A. Trujillo, J. X. Luu, Population and size distribution of small jovian trojan asteroids, *The Astronomical Journal* 120(20) (2000) 1140–1147.
- [3] S. Kemp, An examination of the mass limit for stability at the triangular lagrange points for a three-body system and a special case of the four-body problem, Master's Theses.
URL [http://scholarworks.sjsu.edu/etd_theses/4546](http://scholarworks.sjsu.edu/etd/_theses/4546)
- [4] Wikipedia contributors, Lagrangian point — Wikipedia, the free encyclopedia, https://en.wikipedia.org/w/index.php?title=Lagrangian_point&oldid=891210074, [Online; accessed 29-April-2019] (2019).
- [5] F. Yoshida, T. Nakamura, Size distribution of faint jovian l4 trojan asteroids, *The Astronomical Journal* 130 (6) (2005) 2900–2911. doi:10.1086/497571.
URL <https://doi.org/10.10862F497571>
- [6] A. Celletti, A. Giorgilli, On the stability of the lagrangian points in the spatial restricted problem of three bodies, *Celestial Mechanics and Dynamical Astronomy* 50 (1991) 31–58.
- [7] B. Sicardy, Stability of the triangular Lagrange points beyond Gascheau's value, *Celestial Mechanics and Dynamical Astronomy* 107 (2010) 145–155. doi:<http://dx.doi.org/10.1002/andp.19053221004>.

Appendix A. Program Run-Times

Figure	Integrator Used	Run Time /s (3s.f.)
4(a-d)	dopri5	0.324
5(a)	odeint	18.2
5(b)	odeint	18.3
6	odeint	151
7	odeint	183
8	odeint	46.8
9(a)	lsoda	125
10(a)	odeint	210
10(b)	lsoda	261
11(a)	odeint	232
11(b)	lsoda	255
12	lsoda	632
13	odeint	351
14(a)	odeint	260
14(b)	odeint	281
15(a-b)	dopri5	4.33
16(a)	dopri5	86.4
16(b)	dopri5	112

Table A.3: Integrators used and run times for each figure generated. Some figures have been omitted as negligible. Others (where multiple are referenced) have been averaged due to similarity.